Supporting Information

Distant Protonated Pyridine Groups in Water-Soluble Iron Porphyrin Electrocatalysts Promote Selective Oxygen Reduction to Water

Benjamin D. Matson,[a] Colin T. Carver,[a,b] Amber Von Ruden,[c] Jenny Y. Yang,[c,d] Simone Raugei,[c,e] and James M. Mayer[a,]*

a. Department of Chemistry, University of Washington, Seattle WA USA, 98195-1700. Contact information for JMM: 01-206-553-2083; mayer@chem.washington.edu.

b. Current address: Intel Corporation Mail Stop RA3-252 Hillsboro, OR, USA, 97124

c. Pacific Northwest National Laboratory, Richland WA USA.

d. Current address: Joint Center for Artificial Photosynthesis, California Institute of Technology, Mail Code 139-74, Pasadena, CA USA 91125, jyy@caltech.edu.

e. Simone.Raugei@pnnl.gov

Contents:

1. General experimental considerations

Tetrakis(2-pyridyl)porphine chloride was prepared by literature methods[1] from by adding pyrrole and 2-pyridinecarboxaldehyde to refluxing propanoic acid. After solvent removal *in vacuo,* the purple solid was purified by column chromatography and characterized by comparison of its ^{1}H NMR spectrum to that reported in the literature.[2] Tetrakis(4-pyridyl)porphine chloride was purchased from TCI America and used without purification. Metal insertion into both porphyrin systems was done by refluxing the porphine with an excess of $FeCl_2 \cdot 4H_2O$ in DMF for 3 hours and isolated by removing the DMF *in vacuo*, as per literature procedures,[3] and were characterized by ^{1}H NMR spectroscopy. The corresponding triflate salts were prepared by stirring the appropriate catalyst with one equivalent of silver triflate in chloroform for compound **1** and pyridine for compound **2**, with solvent choices dictate by the solubility of the compound. Successful counter-ion substitution was evidenced by the presence of a solid precipitate, assumed to be AgCl. After solvent removal, the solid mixture of catalyst and AgCl was dissolved in 0.5 M HOTf and the insoluble AgCl was isolated by vacuum filtration. The use of DMF and/or pyridine as a solvent produced a tar-like solid upon solvent removal. Vigorous stirring of the tar in water for a period of several hours produced a fine purple powder when isolated by vacuum filtration. No indication of demetallation of **1** or **2** in acid solutions was seen in ^{1}H NMR or optical spectra, consistent with a previous study.[4]

2. General electrochemical considerations

All electrochemical measurements were made on either a BASI Epsilon bipotentiostat (www.bioanalytical.com) or a CH Instruments Model 600D potentiostat (www.chinstruments.com). CV measurements were collected using a 3 mm diameter glassy carbon working electrode, a platinum wire auxiliary, and a Ag/AgCl (Sat'd $KCl_{(aq)}$) reference electrode. Rotating ring-disk voltammetry measurements were collected with a Pine Instruments model AFMSRCE electrode rotator with speed control, using a 5 mm diameter glassy carbon disk working electrode, a Pt ring secondary working electrode (electrode model number AFE6R1PT), a Pt coil auxiliary electrode, and Ag/AgCl (Sat'd $KCl_{(aq)}$) reference electrode. The potentials shown in all figures are referenced to NHE, using Ag/AgCl = -0.197 V vs. NHE.

High Pressure Measurement Considerations:

Measurements involving oxygen pressures above atmospheric pressure were collected in a glass-sleeved stainless steel high-pressure vessel purchased from Parr Instrument Company (http://www.parrinst.com/) utilizing a 3000-psi rupture disk. Measurements with oxygen pressures between 300 and 2000 psi were collected by direct connection to a high pressure O_2 tank with 1/8 inch outside diameter stainless steal tubing from Swagelok (http://swagelok.com/home.aspx) with a wall thickness of 0.028 inches and pressure rating of 8000 psig (part number SS-T2-S-028-20). The Swagelok tubing was connected directly to the same high-pressure vessel and pressure readings were obtained from the vessel's pressure meter.

(1) (a) T. Kaufmann, B. Shamsai, R. S. Lu, R. Bau, G. Miskelly *Inorg. Chem.* 1995, **34**, 5073-5079. (b) K. Kalyansundaram. *Inorg. Chem.* 1984, **23**, 2453-2459.
(2) I. Saltsman, M. Botoshansky, Z. Gross. *Tetrahedron Lett*. 2008, **49**, 4163-4166.
(3) A. D. Adler, F. R. Longo, F. Kampas, J. Kim, *Inorg. Nucl.* 1970, **32**, 2443-2445.
(4) C. Shi and F. C. Anson, *Inorg. Chem.* 1990, **29**, 4298.

The potentiostat leads were attached via a 4 wire feed-through from Conax Technologies (http://www.conaxtechnologies.com/default.aspx).

Analysis of the rotating ring-disk voltammetry (RRDV) data was done according to the method of Lefévre and Dodelet,[4] which relates the ratio of the disk to ring current to the ratio of products formed according to the proposed scheme in Figure S1.

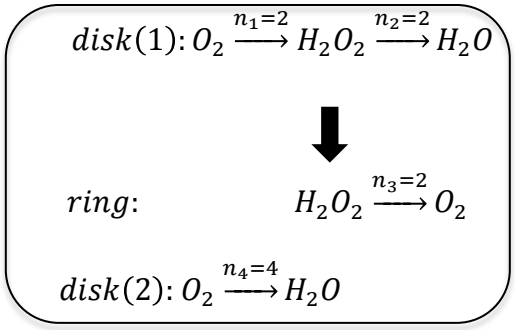

Figure S1. Proposed scheme for the two-pathway reduction of oxygen observed in RRDV measurements.

Based on the observed disk and ring currents (i_{disk} and i_{ring} respectively) and the collection efficiency N (measured to be 0.22 based on ferricyanide RRDV), the percent hydrogen peroxide produced and the average number of electrons transferred can be calculated using the following equations provided by Lefèvre and Dodelet[5].

$$\%H_2O_2 = \frac{100\left(\frac{2i_{ring}}{N}\right)}{i_{disk}+\frac{i_{ring}}{N}} \qquad \text{(S1)}$$

$$n = \frac{4i_{disk}}{i_{disk}+\frac{i_{ring}}{N}} \qquad \text{(S2)}$$

3. Determination of Turnover Frequency

Following the method of Saveànt,[6] turnover frequency (TOF) can be calculated under conditions where the rate is limited by chemical steps and not by electron transfer or substrate diffusion (the so-called 'pure kinetic zone'). In this regime, the TOF can be obtained from the ratio of the catalytic current (i_c) to the peak CV current in the absence of catalysis (i_p), eq 3.

$$\frac{i_c}{i_p} = \frac{n_c}{0.447 \cdot n_p} \cdot \sqrt{\frac{RT}{n_p F}} \cdot \sqrt{\frac{TOF}{\upsilon}} \qquad \text{(S3)}$$

In this equation, n_c = 3.8 (the number of electrons per turnover, determined from the RRDV experiments below), n_p = 1 (the number of e^- in the non-catalytic couple), and υ is the scan rate in V/s. The pure kinetic zone is found at high substrate/catalyst ratios and slow scan rates. It is marked by the catalytic CVs being *S*-shaped rather than peaked and independent of scan rate (rather than typical diffusion limited $i \propto \upsilon^{1/2}$).

(5) M. Lefèvre, J.P. Dodelet, *Electrochim. Acta* 2003, **48**, 2749-2760.
(6) (a) J.M. Savéant, *Chem. Rev.,* 2008, **108**, 2348-2378. (b) Savéant, J. M.; Vianello, E, *Electrochim. Acta* **1965**, *10*, 905-920. (c) Savéant, J. M.; Vianello, E, *Electrochim. Acta* **1967**, *12*, 629-646. (d) Nicholson, R. S.; Shain, I. *Anal. Chem.* **1964**, *36*, 706.

3. ^{1}H NMR spectra

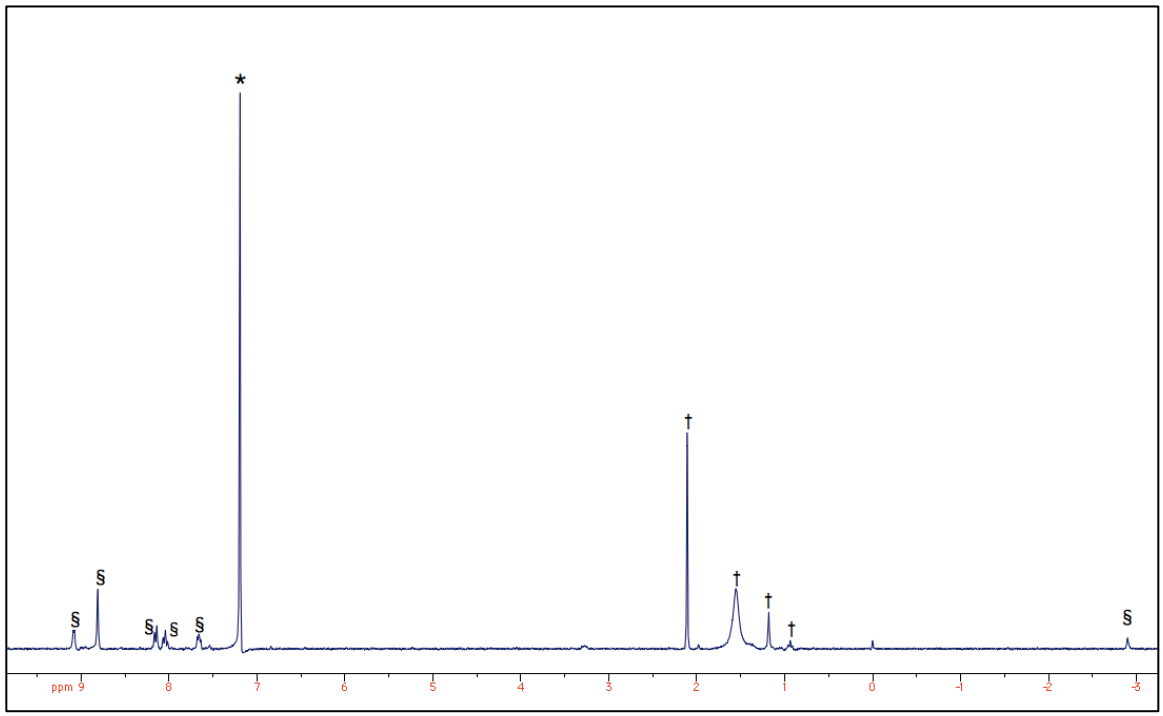

Figure S2. ^{1}H NMR of *meso*-tetra(2-pyridyl)porphine in $CDCl_3$ (*, δ 7.20). Porphyrin peaks (§) were matched to literature spectra;[2] †-marks various impurities.

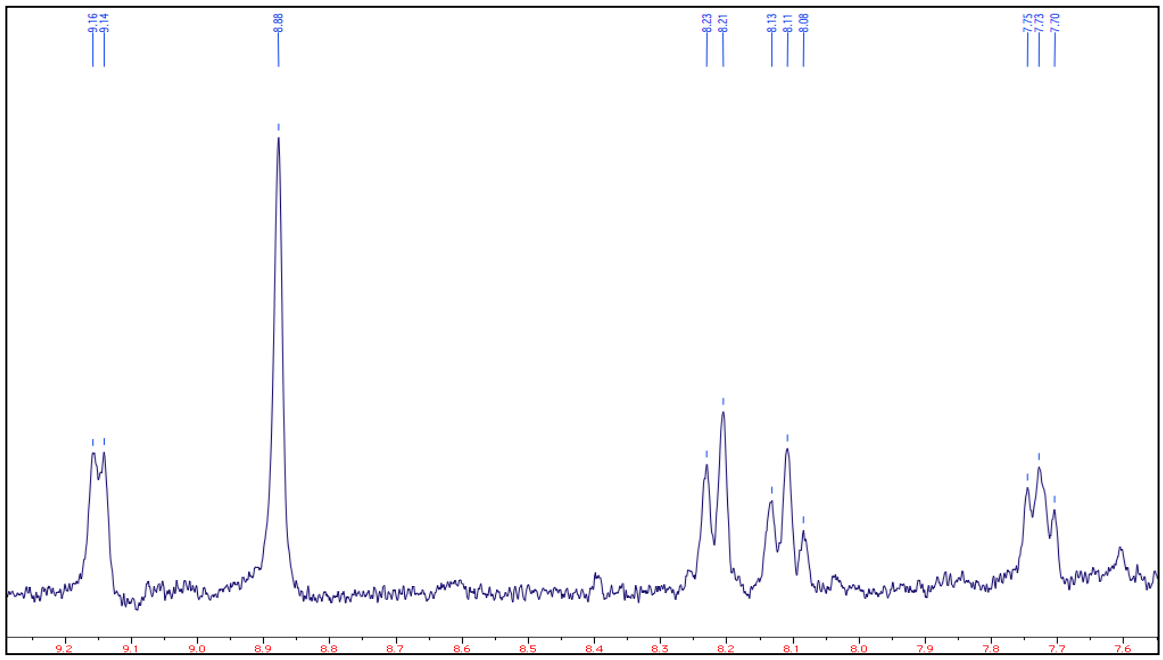

Figure S3. Expansion of the aromatic region of the spectrum in Figure S1.

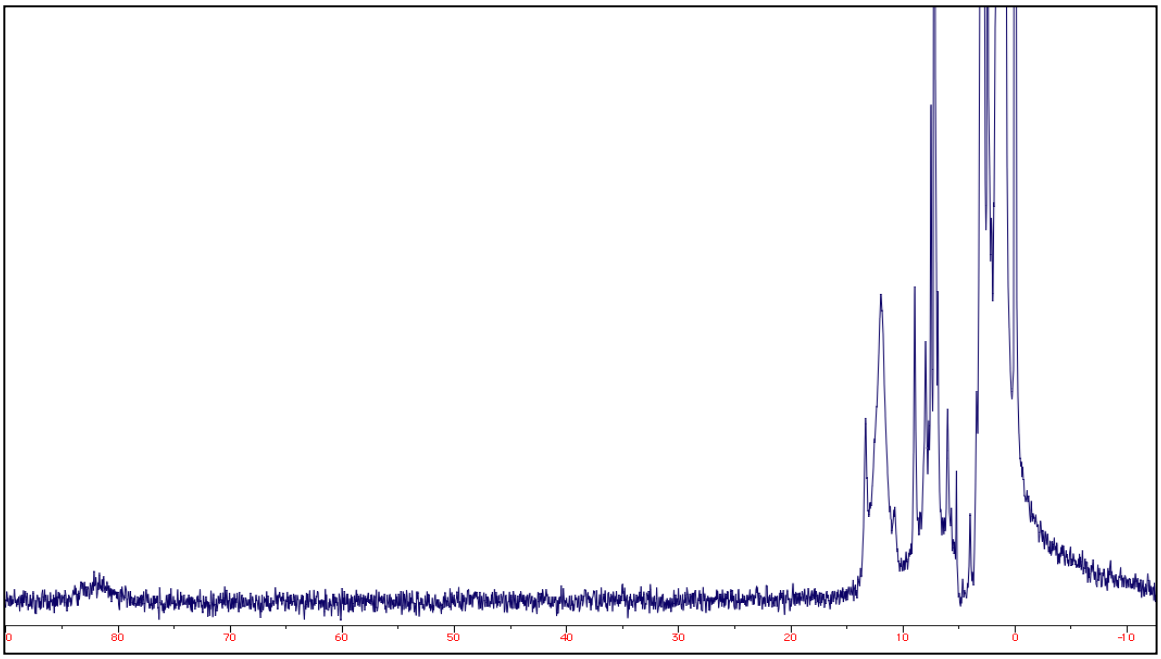

Figure S4. ^{1}H NMR spectrum of Fe(III)-*meso*-tetra(2-pyridyl)porphine chloride **(1)** in $CDCl_3$.

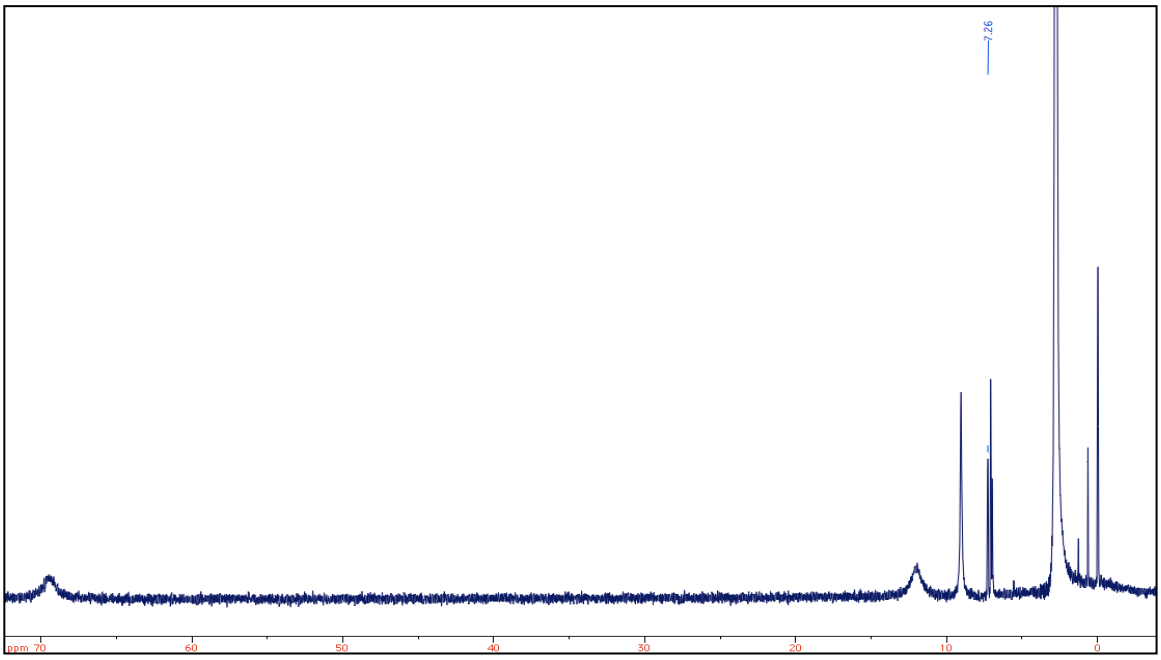

Figure S5. ^{1}H NMR spectrum of Fe(III)-meso-tetra(4-pyridyl)porphine chloride **(2)** in D_2O/D_2SO_4.

4. CV Data

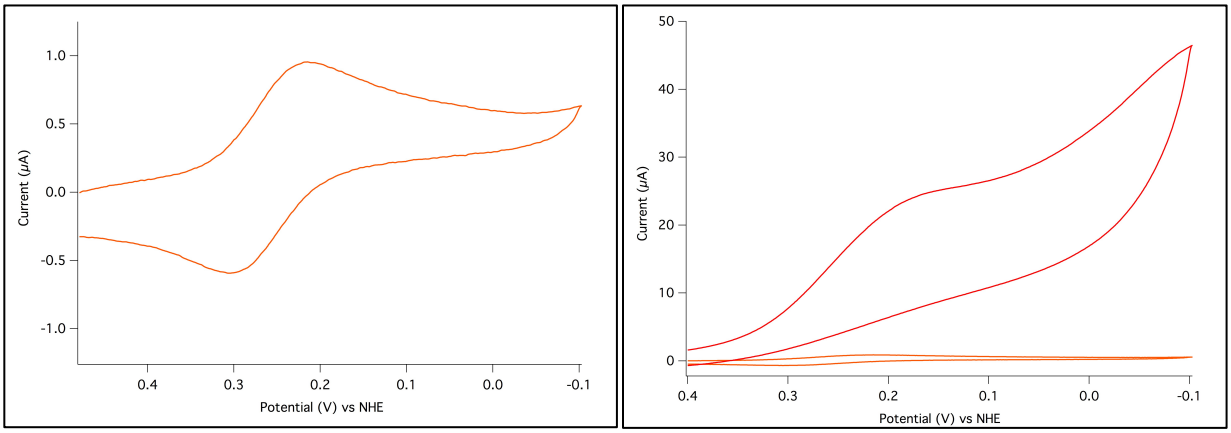

Figure S6. Cyclic voltammograms of **1** (0.30 mM, 0.5 M HOTf) under N_2 gas (left panel and right panel, lower orange curve) and of the same solution under 1 atm O_2 (right panel, red curve, 1.3 mM O_2).

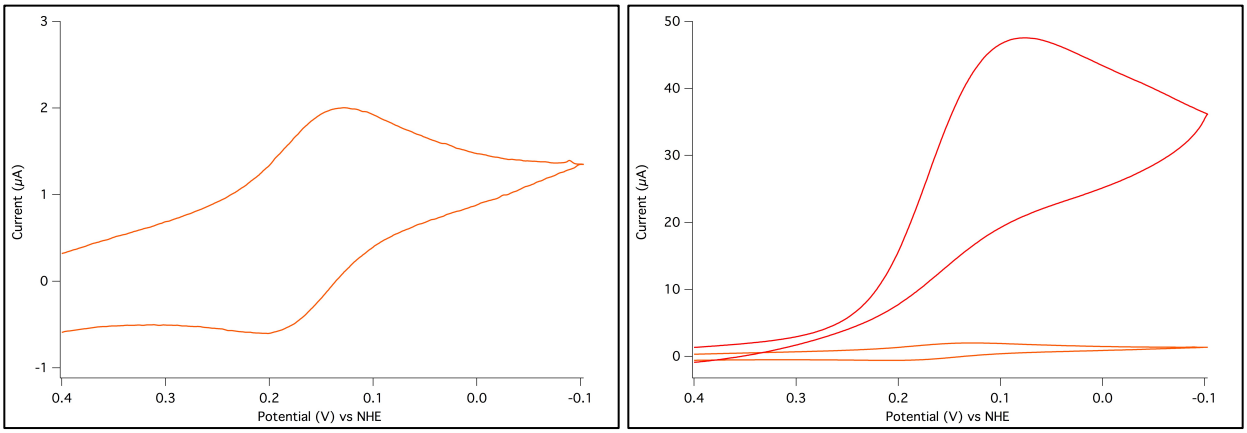

Figure S7. Cyclic voltammograms of **2** (0.30 mM, 0.5 M HOTf) under N_2 gas (left panel and right panel, lower orange curve) and the same solution under 1 atm O_2 (right, red curve, 1.3 mM O_2).

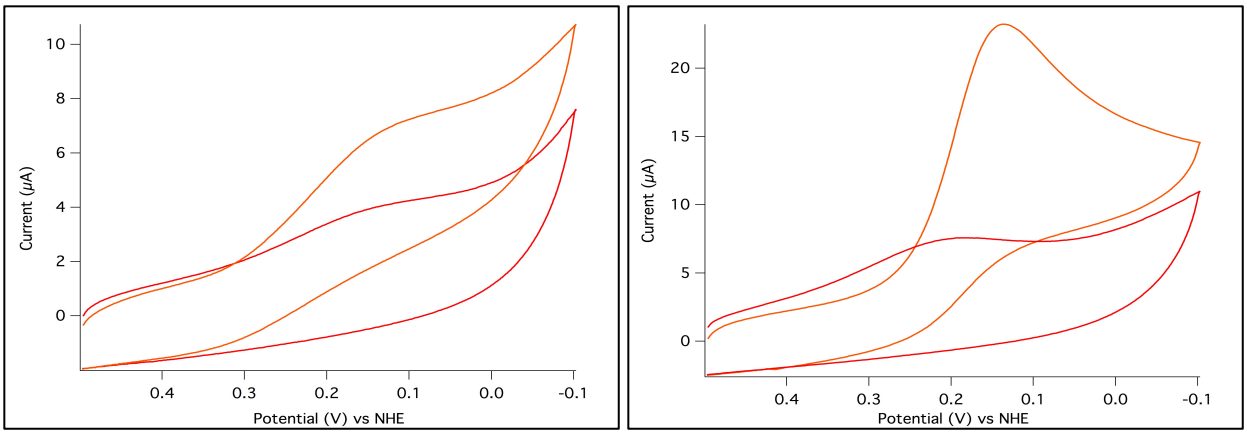

Figure S8. Cyclic voltammograms of **1** (left) and **2** (right) in air (0.27 mM O_2). Orange traces are CVs of solutions of **1** or **2** (0.30 mM catalyst) in 0.5 M HOTf. The electrode was then removed from the solution, rinsed with deionized water but without polishing the glassy carbon electrode, and placed in a 0.5 M HOTf solution with no catalyst; the resulting CVs are shown as the red traces. After correction for the sloping baselines, the in the rinsed cases are significantly lower than those in solutions of **1** or **2**. The catalytic currents in for the rinsed electrodes is attributed to catalyst adsorption onto glassy carbon.

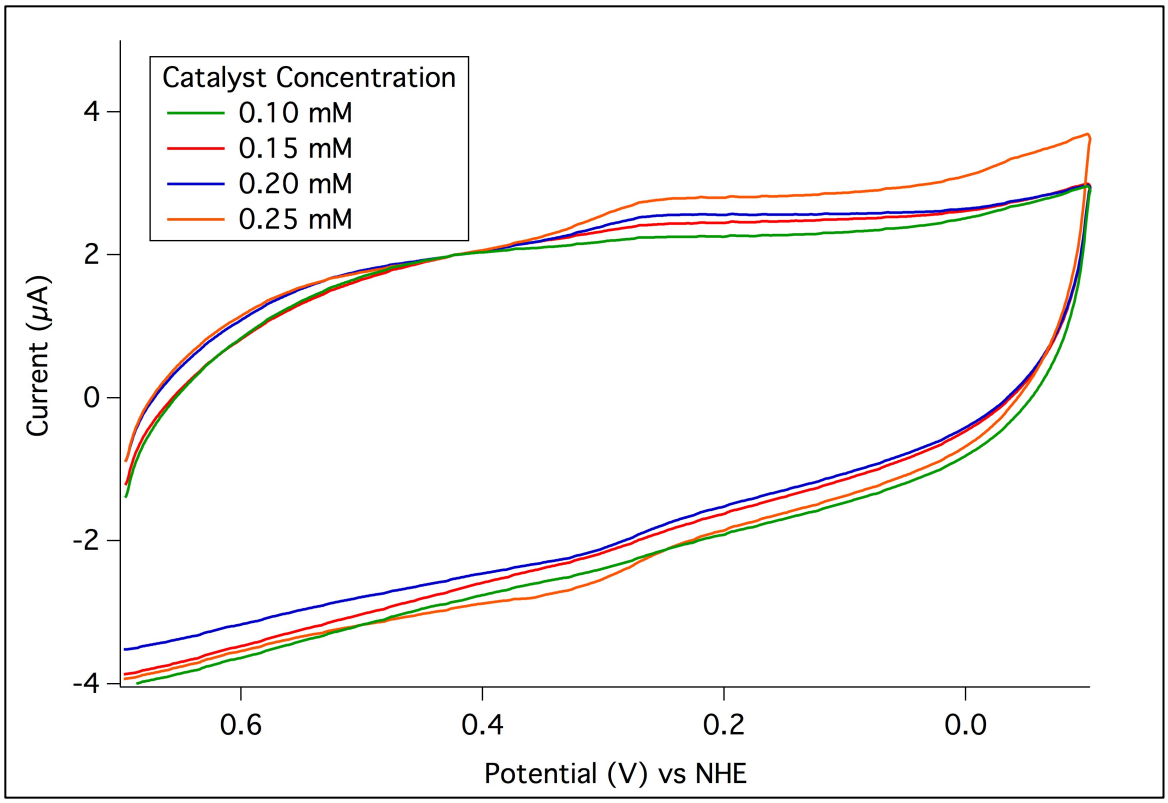

Figure S9. Cyclic voltammograms of **1** (in 0.5 M HOTf) at varying concentrations (as labeled) under 1 atm N_2 gas.

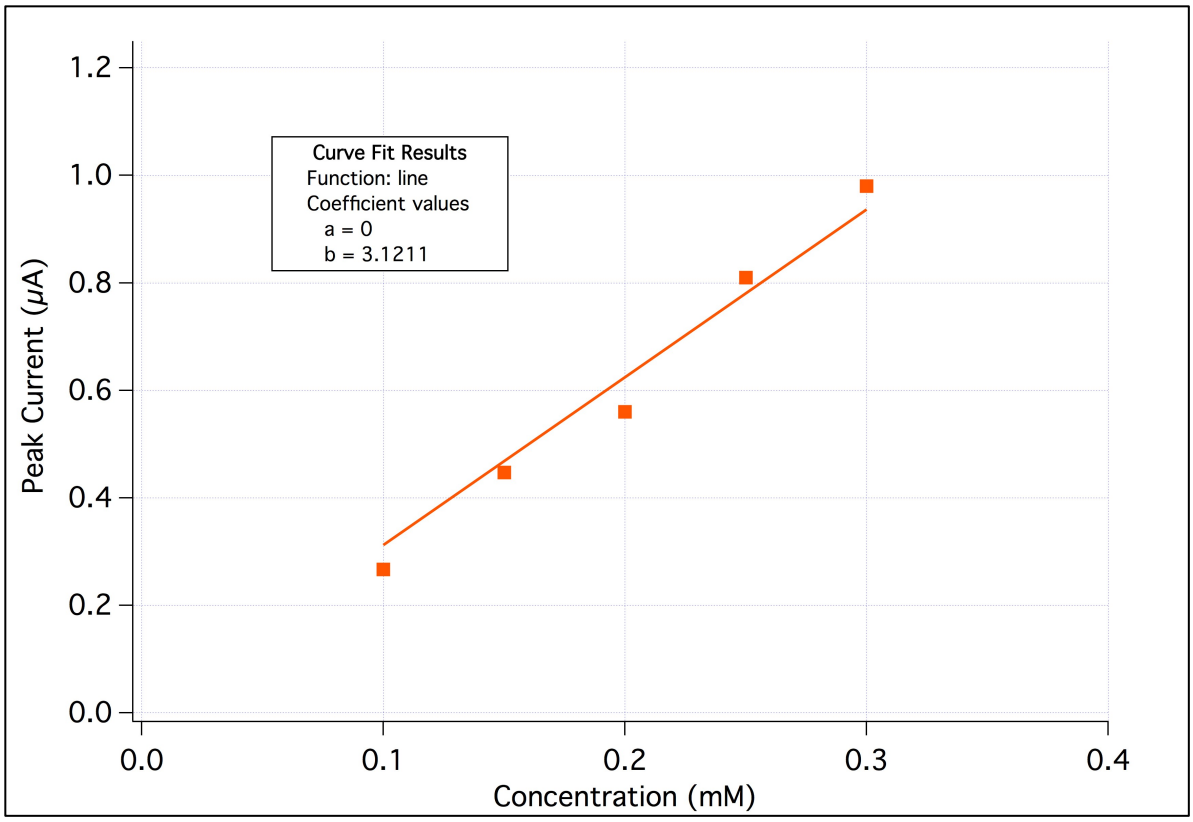

Figure S10. Plot of peak current vs. catalyst concentration using the data shown in Figure S9. Peak current is taken as the current above background at a potential of +220 mV vs. NHE. Concentrations were obtained by dilution of a 0.30 mM stock solution.

5. High Pressure CV Data

None of the voltammograms in this section are background corrected.

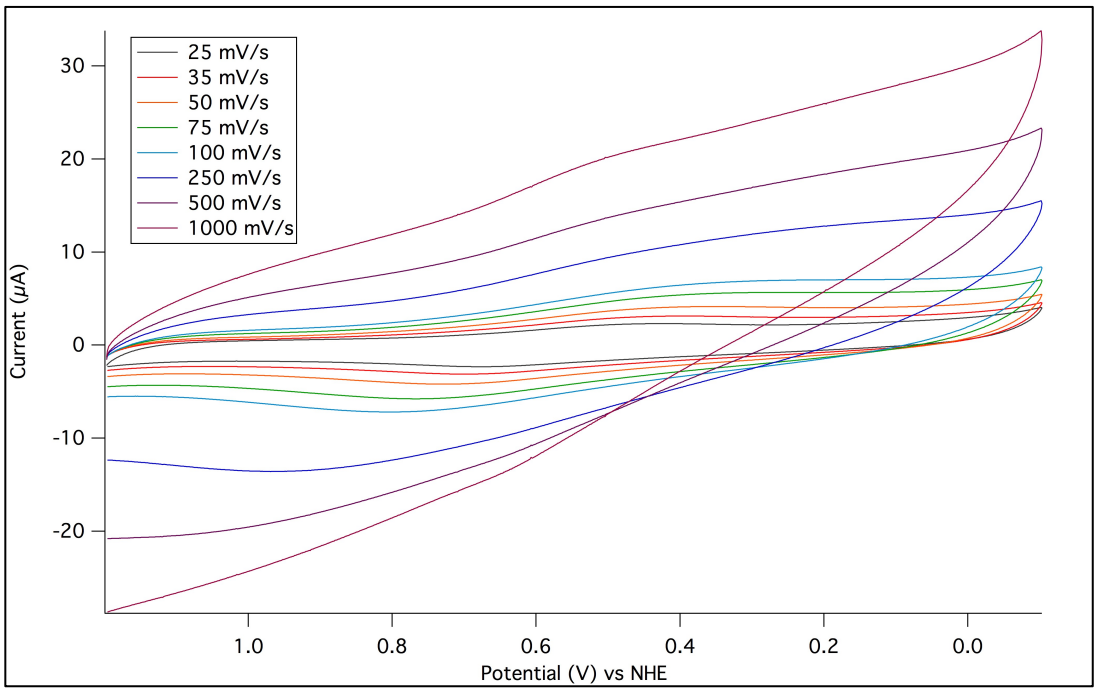

Figure S11. CVs of 0.5 M HOTf under high pressure of O_2 (68 atm, 88 mM) in the absence of any added catalyst, shown at various scan rates (as labeled).

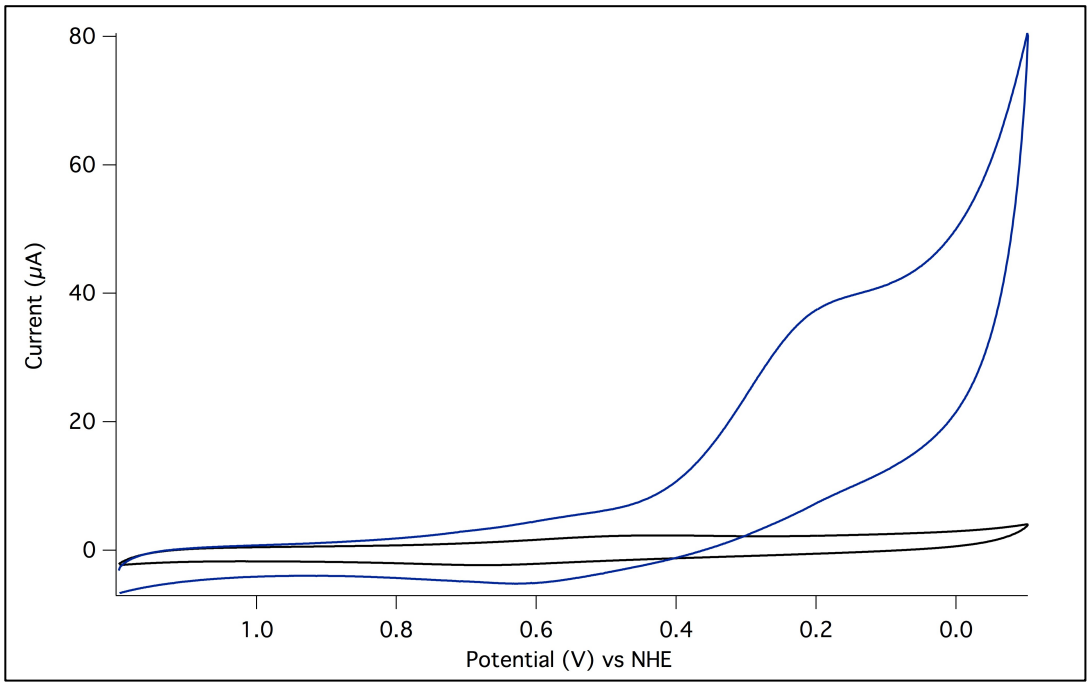

Figure S12. CVs of 0.5 M HOTf (black) and **1** (blue, 0.10 mM, 0.5 M HOTf) under high pressure of O_2 (68 atm, 88 mM) at a scan rate of 25 mV/s.

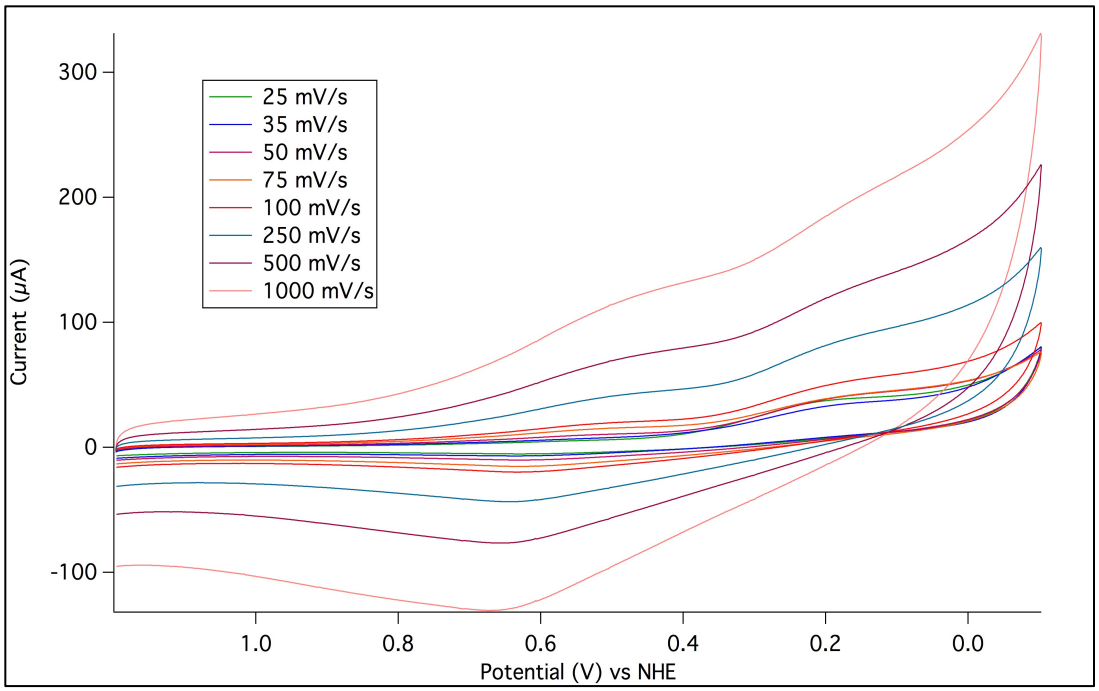

Figure S13. CVs of **1** (0.10 mM, 0.5 M HOTf) under high pressure of O_2 (68 atm, 88 mM) at various scan rates (as labeled). Note the much larger vertical scale than the background scan in Figure S11.

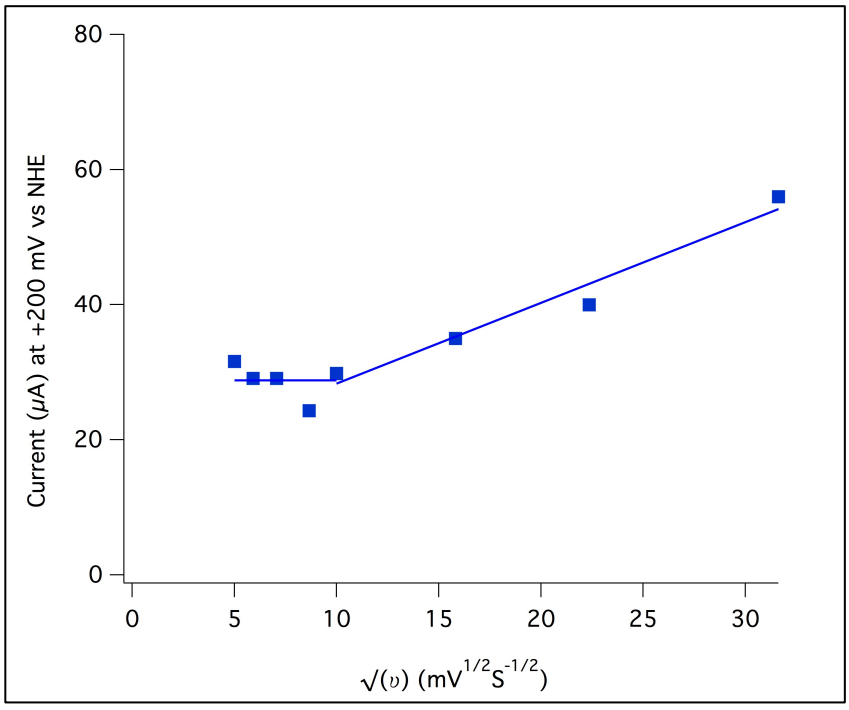

Figure S14. Plot of current above background at +200 mV *vs.* square root of scan rate as taken from Figure S13.

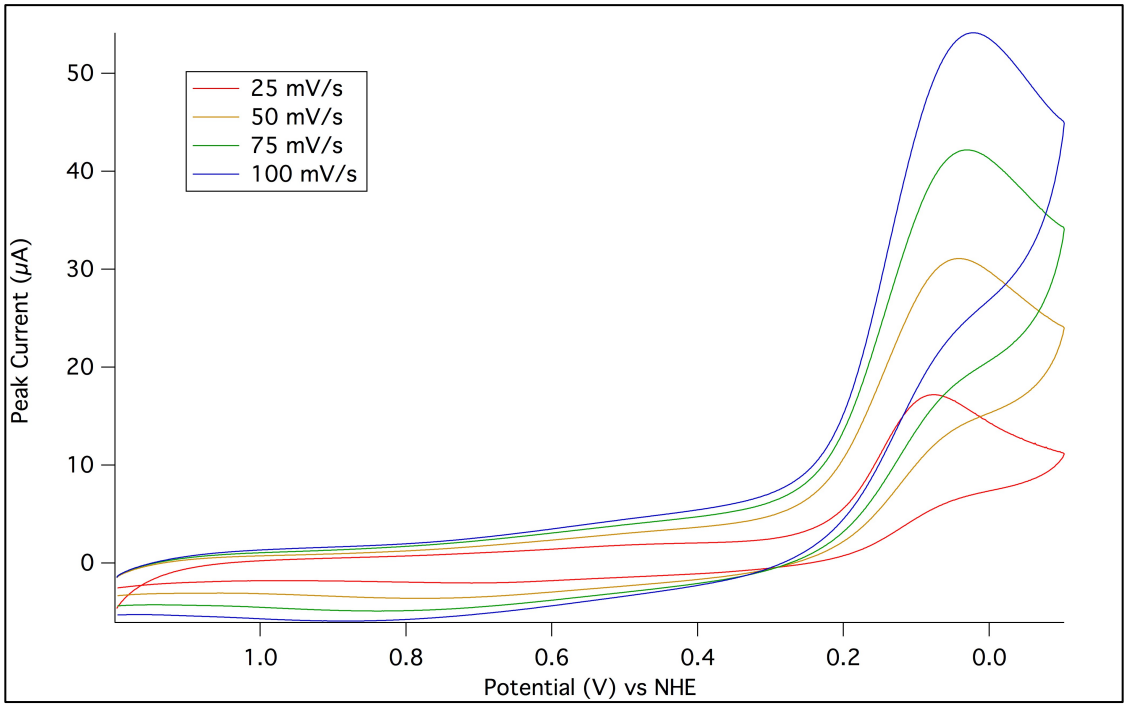

Figure S15. CVs of **2** (0.10 mM, 0.5 M HOTf) under high pressure of O_2 (68 atm, 88 mM) at various scan rates (as labeled).

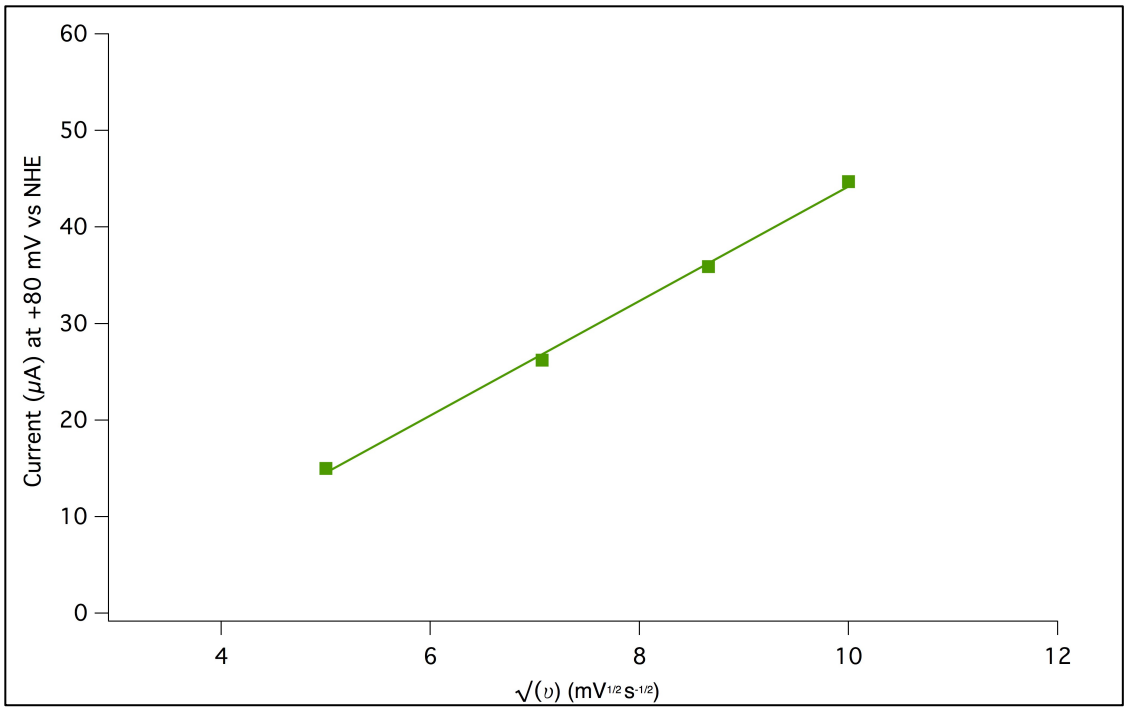

Figure S16. Plot of current above background at +80 mV vs. square root of scan rate as taken from Figure S15.

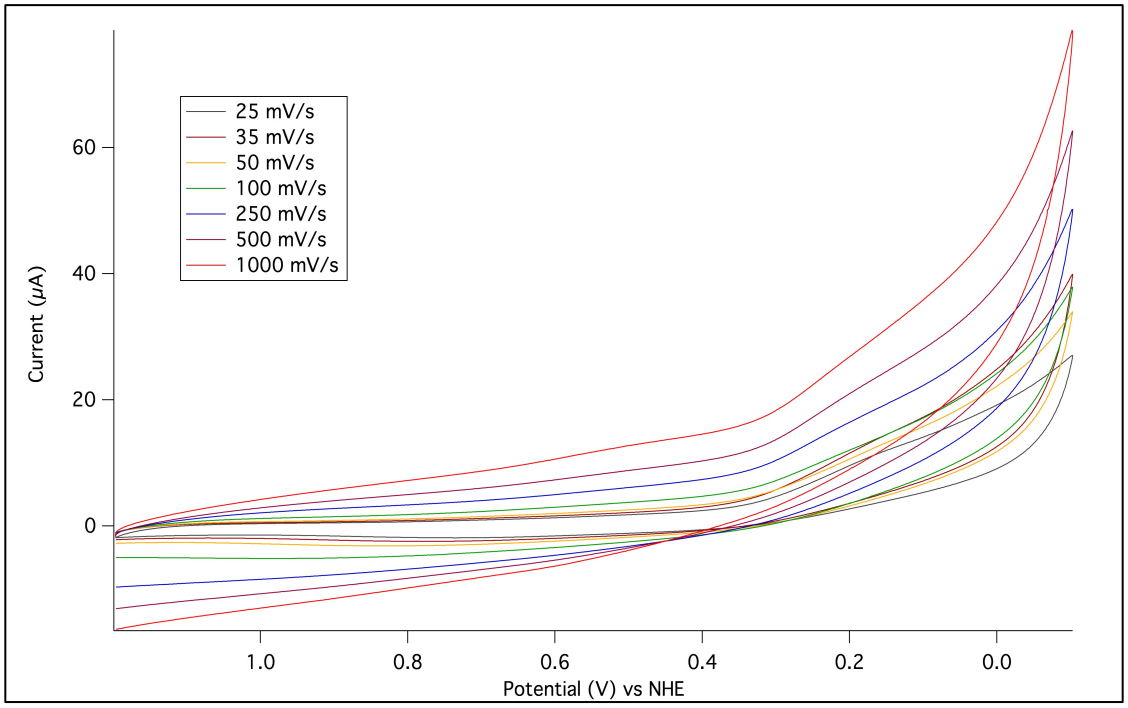

Figure S17. CVs of **1** (0.10 mM, 0.25 M HOTf) under high pressure of O_2 (68 atm, 88 mM) at various scan rates (as labeled). This is the same experiment as in Figure S13 except for a factor of two lower acid concentration.

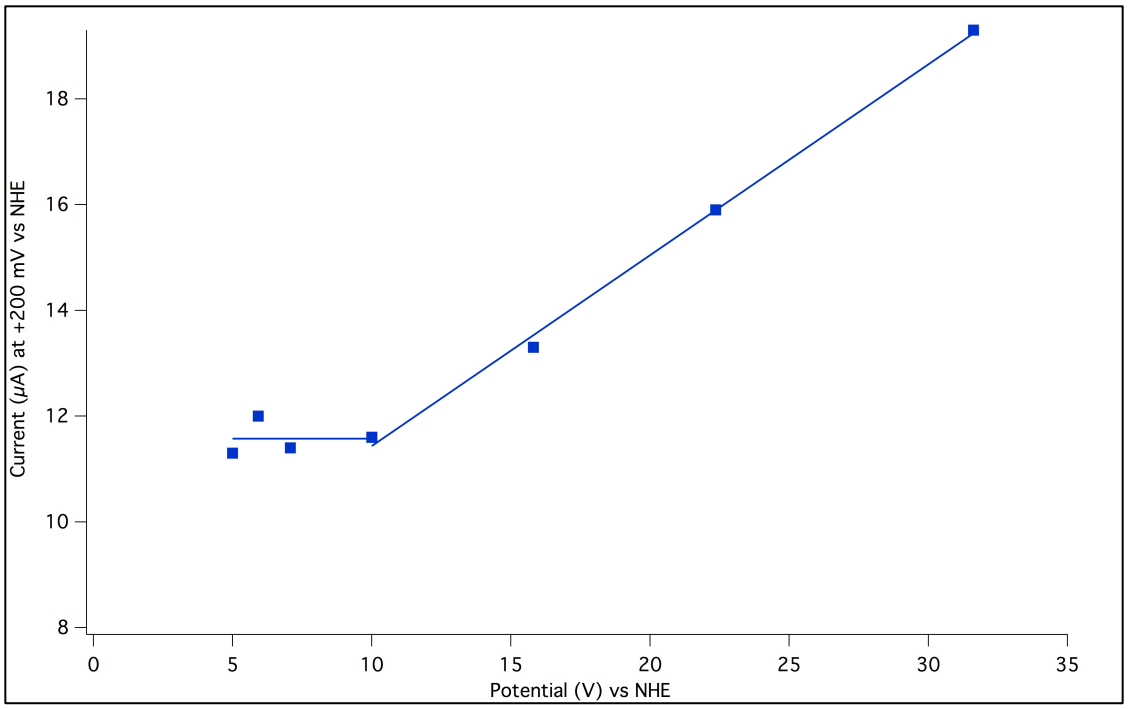

Figure S18. Plot of current above background at +200 mV vs. square root of scan rate as taken from Figure S17.

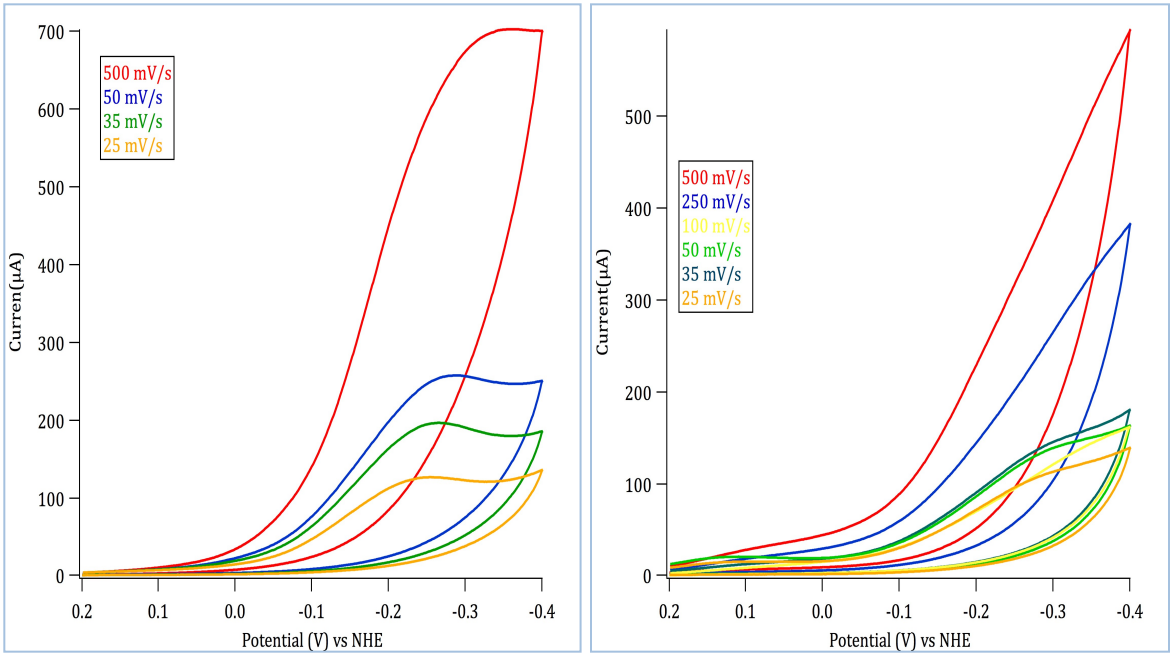

Figure S19. CVs of **1Cl** (left) and **2Cl** (right) under high O_2 pressure 2300 psi (0.01 mM cat., 0.5 M KCl, 0.25 M HCl, 155 mM O_2).

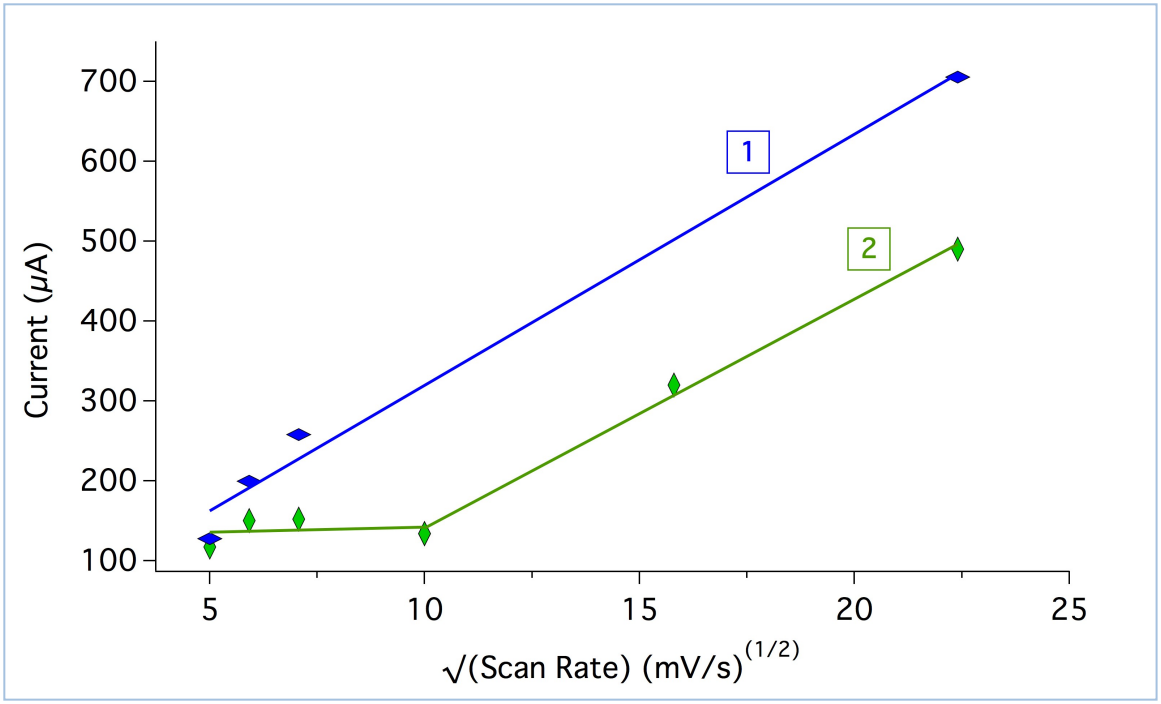

Figure S19. Peak current at -250 mV vs. NHE plotted against the square root of scan rate for **1Cl** and **2Cl** using the data from Figure S18.

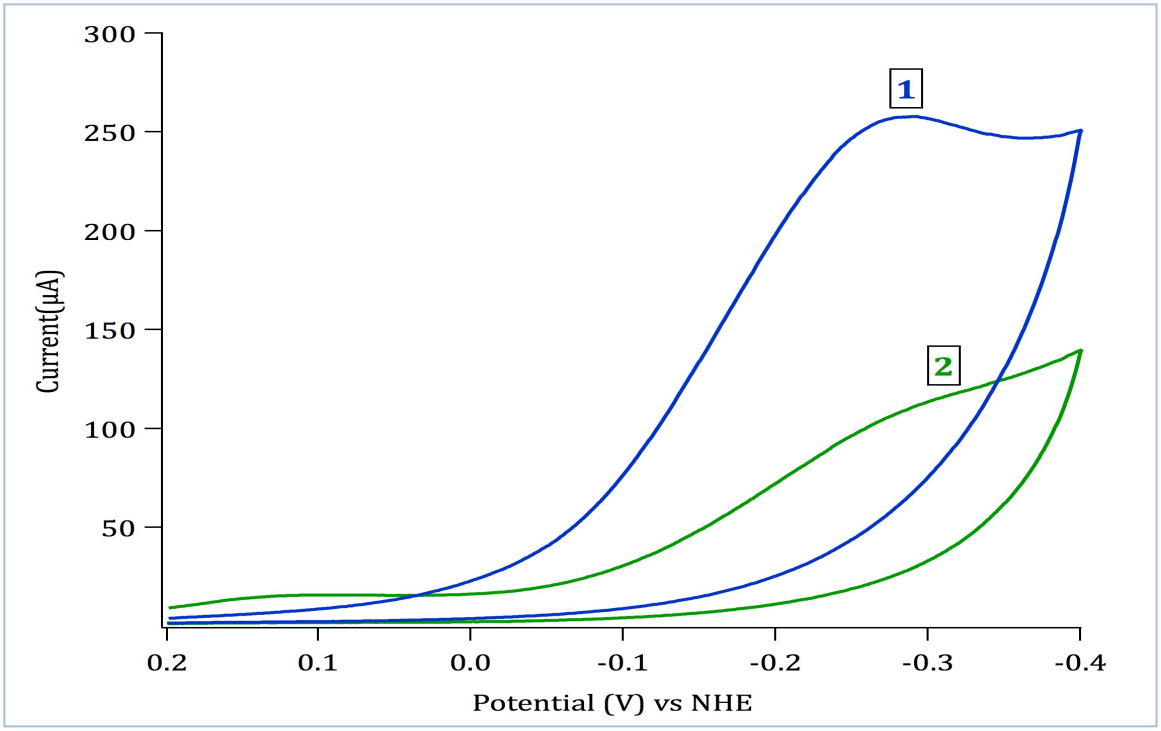

Figure S20. Comparison of CVs of **1Cl** and **2Cl** at 50 mV/s (0.01 mM catalyst, 0.5 M KCl 0.25 M HCl, 2300 psi, 155 mM O_2).

6. Rotating Ring-Disk Voltammetry

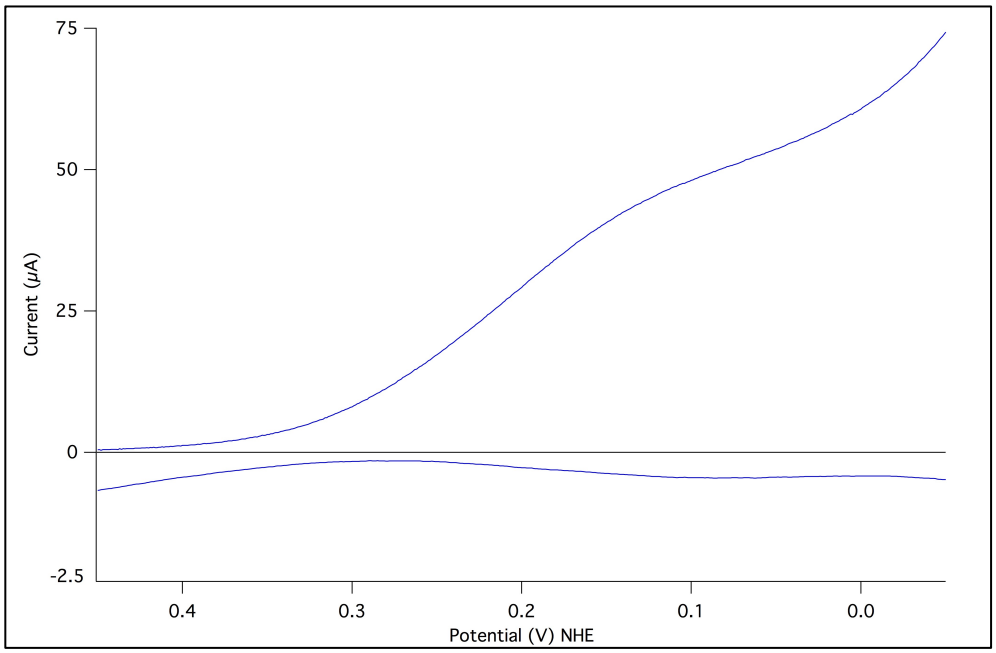

Figure S21. Rotating Ring-Disk Voltammogram of **1** (0.3 mM) in 0.5 $HOTf_{(aq)}$ under atmospheric conditions (1 atm air; 0.27 mM O_2). Ring Potential: 1.19 V vs. NHE, Rotation Rate: 2000 rpm, scan rate: 250 mV/s. Note that i_{ring} is shown 10X magnified.

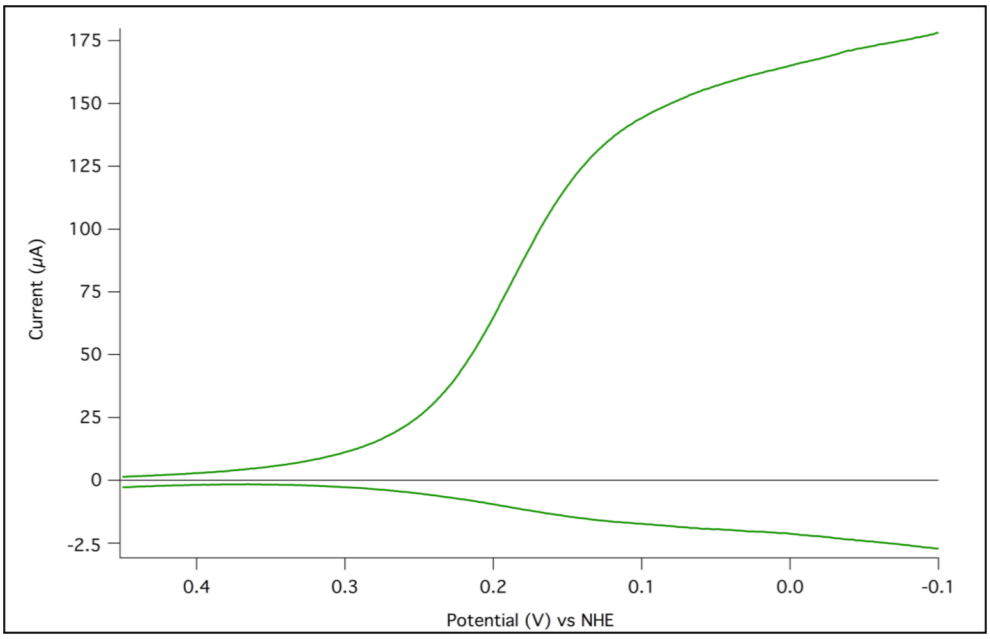

Figure S22. Rotating Ring-Disk Voltammogram of **2** (0.3 mM) in 0.5 $HOTf_{(aq)}$ under atmospheric conditions (1 atm air; 0.27 mM O_2). Ring Potential: 1.19 V vs. NHE, Rotation Rate: 2000 rpm, scan rate: 250 mV/s. Note that i_{ring} is shown 10X magnified.

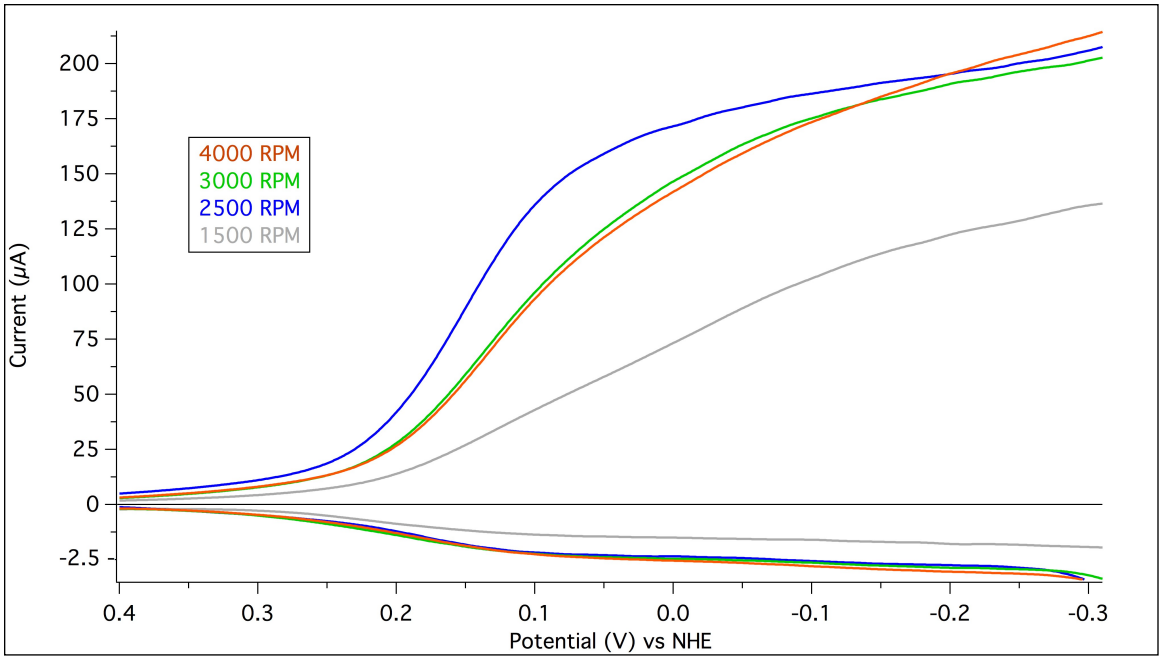

Figure S23. Rotating Ring-Disk Voltammogram of **2Cl** (0.35 mM) in aqueous 0.25 M HCl/0.5 M KCl under 1 atm air (0.27 mM O_2). Ring Potential 1.19 V vs. NHE; rotation Rates as shown.

8. *Ab initio* Calculations.

Structures were optimized using the PBE functional.[7] A triple-zeta basis set augmented with two sets of d-type and p-type polarization functions was employed for the valence electrons of all the atoms, except the Fe atom for which a double zeta basis set with polarization function was used.[8] The interaction between valence and core electrons was described using norm-conserving pseudopotentials.[9] The electrostatic energy was calculated using an auxiliary planewave basis set with a cut-off energy of 280 Ry in 30 Å periodic cubic box.[10] Calculations were performed with the CP2K code.[14]

The pK_a calculations were carried out using the B3P86 functional[11] using the isodesmic scheme reported in Ref. 12. The pK_a of 5.25 for the pyridinium cation in aqueous solution was used as reference for the isodesmic calculation. All electrons calculation were performed using the Stuttgart–Dresden relativistic effective core potential and associated basis set (SDD) for Fe, the 6-311G** basis set of O, N and the protic hydrogens, and the 6-31G* for all of the other atoms. Harmonic vibrational frequencies were calculated at the optimized structures using the same level of theory to estimate the zero-point energy and thermal contributions (T = 298K and P = 1 bar) to the gas-phase free energy. Solvation free energies were then computed using a self-consistent reaction field model at the same level of theory as for the other steps. The continuum polarizable conductor model[13] was used with Bondi radii.[14] These calculations were carried out with the program Gaussian 09.[15]

(7) J. P. Perdew, K. Burke, M. Ernzerhof, *Phys. Rev. Lett.* **1997**, *78*, 1396.
(8) J. VandeVondele, J. Hutter, *J. Chem. Phys.* **2007**, *127*, 114105.
(9) S. Goedecker, M. Teter, J. Hutter, *Phys. Rev. B* **1996**, *54*, 1703.
(10) J. VandeVondele, M. Krack, F. Mohamed, M. Parrinello, T. Chassaing, J. Hutter, *Comput. Phys. Commun.* **2005**, 167, 103 (www.cp2k.org).
(11) (a) J. P. Perdew, *Phys. Rev. B* **1986**, *33*, 8822. (b) A. D. Becke, *J. Chem. Phys.* **1993**, *98*, 5648.
(12) C. L. Chen, R. J. Rousseau, S. Raugei, M. Dupuis, D. L. Dubois, R. M. Bullock, *Organometallics* **2011**, *30*, 6108.
(13) M. Cossi, N. Rega, G. Scalmani, V. Barone, *J. Comput. Chem.* **2003**, *24*, 669.
(14) A. Bondi, *J. Phys. Chem.* **1964**, *68*, 441.
(15) Gaussian 09, Revision B.01, M. J. Frisch, G. W. Trucks, H. B. Schlegel, G. E. Scuseria, M. A. Robb, J. R. Cheeseman, G. Scalmani, V. Barone, B. Mennucci, G. A. Petersson, H. Nakatsuji, M. Caricato, X. Li, H. P. Hratchian, A. F. Izmaylov, J. Bloino, G. Zheng, J. L. Son- nenberg, M. Hada, M. Ehara, K. Toyota, R. Fukuda, J. Hasegawa, M. Ishida, T. Nakajima, Y. Honda, O. Kitao, H. Nakai, T. Vreven, J. A. Montgomery, Jr., J. E. Peralta, F. Ogliaro, M. Bearpark, J. J. Heyd, E. Brothers, K. N. Kudin, V. N. Staroverov, R. Kobayashi, J. Normand, K. Raghavachari, A. Rendell, J. C. Burant, S. S. Iyengar, J. Tomasi, M. Cossi, N. Rega, J. M. Millam, M. Klene, J. E. Knox, J. B. Cross, V. Bakken, C. Adamo, J. Jaramillo, R. Gomperts, R. E. Stratmann, O. Yazyev, A. J. Austin, R. Cammi, C. Pomelli, J. W. Ochterski, R. L. Martin, K. Morokuma, V. G. Zakrzewski, G. A. Voth, P. Salvador, J. J. Dannenberg, S. Dapprich, A. D. Daniels, O. Farkas, J. B. Foresman, J. V. Ortiz, J. Cioslowski, D. J. Fox, Gaussian, Inc., Wallingford CT, 2009.